SIMULATIONS OF NONLINEAR PLATE DYNAMICS: AN ACCURATE AND EFFICIENT MODAL ALGORITHM

Michele Ducceschi, *

Acoustics and Audio Group,
University of Edinburgh,
Edinburgh, UK
`v1mducce@exseed.ed.ac.uk`

Cyril Touzé,

IMSIA, ENSTA ParisTech, CNRS, CEA, EDF,
Université Paris-Saclay,
Palaiseau Cedex, France
`cyril.touze@ensta-paristech.fr`

ABSTRACT

This paper presents simulations of nonlinear plate vibrations in relation to sound synthesis of gongs and cymbals. The von Kármán equations are shown and then solved in terms of the modes of the associated linear system. The modal equations obtained constitute a system of nonlinearly coupled Ordinary Differential Equations which are completely general as long as the modes of the system are known. A simple second-order time-stepping integration scheme yields an explicit resolution algorithm with a natural parallel structure. Examples are provided and the results discussed.

1. INTRODUCTION

Nonlinear vibrations of plates constitute a large domain of research which embraces fields ranging from mechanical and civil engineering, to physics and sound synthesis [1, 2, 3, 4, 5]. The latter is the subject of interest in this work, because plates are, geometrically speaking, the simplest kind of *idiophone* although they share the same salient dynamical features of idiophones of more complex shape (bells, shells, gongs). Hence, numerical simulations of plates offer appealing possibilities for sound synthesis with direct applications to the sound of gongs and cymbals. However, because of the complexity of the nonlinear dynamics, time-domain simulations have become a feasible possibility only in recent years, when compared to sound synthesis of simpler systems such as linear bars [6] and plates [7]. The first complete study on full time-domain simulations of the classic nonlinear plate equations (the von Kármán equations) is due to Bilbao [8]. In this work a rectangular plate with simply-supported conditions is considered and a solution given in terms of a stable, second-order, implicit Finite Difference scheme. The stability condition is achieved through numerical conservation of the energy of the system. Subsequent work by Bilbao and Torin extended the case of a single plate to a full 3D multi-plate environment, where the plates are coupled through pressure waves in air [9]. On the other hand, a modal approach was proposed by Chadwick [10] to treat the case of shells. More recently, a modal approach was proposed by these authors to solve the von Kármán plate equations [11]. Such model is based on the projection of the original system onto the linear modes. Time integration is performed using the time-stepping scheme borrowed from Bilbao [8] and adapted to the modal equations so to give energy conservation mode by mode. Such approach, despite not being *per se* "better" than Finite Differences, has anyhow proven useful for a number of reasons, namely

- for particular combinations of geometry and boundary conditions, the modes are known analytically and therefore the coupling coefficients and eigenfrequencies can be calculated with very high precision (the case of a circular plate with a free boundary, notoriously difficult to treat using Finite Differences, falls into this category);

- damping can be implemented mode by mode resulting in a much more accurate (frequency-dependent) representation of losses.

In turn, the modal approach should be regarded as a practical alternative to Finite Differences in the case of plates. In this work, the modal approach is described and some applications shown. With respect to [11], the time-stepping scheme selected in the present work is a simpler Störmer-Verlet scheme instead of the more complex implicit scheme. The simplification obtained through this choice comes at a high cost: the *stability* of the resulting numerical algorithm. It is, of course, the case to stress the importance of numerical stability when dealing with sound synthesis routines: as a general rule, an algorithm design unable to guarantee stability should be frowned upon.

For the case of the nonlinear modal equations in this work, however, an exception will be made. In fact, stable modal and Finite Difference algorithms have been extensively studied in the aforementioned works, and therefore the focus in this paper will be on *efficiency* rather than stability. In addition, the Störmer-Verlet scheme is perfectly adapted to the problem of the *linear* plate, being energy conserving and stable. The choice of this scheme is justified on the basis that

- the resulting algorithm is *explicit* and therefore does not require to solve a linear system of algebraic equations;

- for the modal equations, the calculation of the nonlinear term can be *highly parallelised* thus allowing fast computations.

The paper is composed as follows: in section 2 the equations are presented along with the modal approach. Section 3 presents the Störmer-Verlet integration scheme and resulting algorithm. Section 4 presents two case studies; convergence of the coupling coefficients is shown. Section 5 discusses in more detail the simulations obtained with scheme.

2. MODEL EQUATIONS

The literature presents a number of model equations describing the nonlinear behaviour of plates. Such models rely on different assumptions which simplify the complexity of the system [1]. In

general, the nonlinearity of a plate is of geometric type, meaning that nonlinear effects come into existence when the amplitude of vibrations increases above a reference amplitude. In actual fact, for such high amplitudes, flexural displacements must entail some kind of in-plane motion which results in a coupling of the modes of vibrations. Amongst the many possible models that describe such dynamics, the von Kármán model represents a particularly attractive choice. Such model, in fact, describes with high degree of accuracy the nonlinear dynamics of plates (at least for vibrations up to a few times the thickness), despite a relatively straightforward extension of the underlying linear model (the Kirchhoff plate equation). In the von Kármán model, the in-plane displacement is originated by a second order correction to the linear strain tensor [12]. Such correction results in a modal coupling for the flexural modes. The von Kármán equations for the flexural displacement $w(\mathbf{x}, t)$ are written as

$$\rho h \ddot{w} + D \Delta \Delta w = \mathcal{L}(w, F) + p(\mathbf{x}, t) - R(\dot{w}),$$

$$\Delta \Delta F = -\frac{Eh}{2} \mathcal{L}(w, w),$$

where ρ is the material volume density, h the plate thickness, and D stands for flexural rigidity: $D = Eh^3/12(1 - \nu^2)$, with E and ν respectively Young modulus and Poisson ratio. Δ represents the two-dimensional Laplacian operator, while $p(\mathbf{x}, t)$ stands for the normal external forcing, and $R(\dot{w})$ is a generic expression for the viscous damping depending on the velocity field. The function $F(\mathbf{x}, t)$ is known as *Airy stress function* and it accounts for the in-plane displacement. The operator $\mathcal{L}$ is generally referred to as the *von Kármán operator* or *Monge-Ampère form* in the literature and may be expressed in intrinsic coordinates, for two functions $f(\mathbf{x})$ and $g(\mathbf{x})$, as [13]

$$\mathcal{L}(f, g) = \Delta f \Delta g - \boldsymbol{\nabla}\boldsymbol{\nabla} f : \boldsymbol{\nabla}\boldsymbol{\nabla} g,$$

where : denotes the doubly contracted product of two tensors.

2.1. Modal approach

The von Kármán equations are now solved formally using a *modal approach*. This means that both the transverse and in-plane functions are expanded onto a series of base functions corresponding to the modes of the associated linear system (which form therefore a complete set over the domain of the plate). Note that the following derivation is independent of the choice of the *geometry of the plate* and of the *boundary conditions*. Let $\{\Phi_k(\mathbf{x})\}_{k \geq 1}$ be the eigenmodes of the transverse displacement. These functions are the solutions of the Sturm-Liouville eigenvalue problem

$$\Delta \Delta \Phi_k(\mathbf{x}) = \frac{\rho h}{D} \omega_k^2 \Phi_k(\mathbf{x}), \qquad (2)$$

together with the associated boundary conditions. In Eq. (2), ω_k stands for the kth radian eigenfrequency. The linear modes are defined up to a constant of normalisation that can be chosen arbitrarily. For the sake of generality, S_w denotes the constant of normalisation of the function $\bar{\bar{\Phi}} = S_w \frac{\Phi_k(\mathbf{x})}{\|\Phi_k\|}$. The norm is obtained from a scalar product $< \alpha, \beta >$ between two functions $\alpha(\mathbf{x})$ and $\beta(\mathbf{x})$, defined as

$$< \alpha, \beta > = \int_S \alpha \beta \, \mathrm{d}S \qquad \longrightarrow \qquad \|\Phi_k\|^2 = < \Phi_k, \Phi_k >,$$

where S represents the area of the plate.

The eigenmodes for the Airy stress function are denoted as $\{\Psi_k(\mathbf{x})\}_{k \geq 1}$. They satisfy the following eigenvalue problem

$$\Delta \Delta \Psi_k(\mathbf{x}) = \zeta_k^4 \Psi_k(\mathbf{x}), \qquad (3)$$

together with the associated boundary conditions for F. The linear modes so defined are orthogonal with respect to the scalar product, and are therefore a suitable function basis [14]. Orthogonality between two functions $\Lambda_m(x, y), \Lambda_n(x, y)$ is expressed as

$$< \Lambda_m, \Lambda_n > = \delta_{m,n} \|\Lambda_m\|^2,$$

where $\delta_{m,n}$ is Kronecker's delta.

The Partial Differential Equations (1) for the perfect plate are discretised by expanding the two unknowns w and F along their respective eigenmodes

$$w(\mathbf{x}, t) = S_w \sum_{k=1}^{N_\Phi} \frac{\Phi_k(\mathbf{x})}{\|\Phi_k\|} q_k(t),$$

$$F(\mathbf{x}, t) = S_F \sum_{k=1}^{N_\Psi} \frac{\Psi_k(\mathbf{x})}{\|\Psi_k\|} \eta_k(t),$$

where $q_k(t)$ and $\eta_k(t)$ represent respectively the modal transverse displacement and the modal coordinate for the Airy stress function. The integers N_Φ and N_Ψ are intended to be *finite* for any numerical simulation. Following a standard projection technique and using the orthogonality relationship leads to discretisation of system (1) [15]. The discretised von Kármán equations read

$$\ddot{q}_s + \omega_s^2 q_s + 2\xi_s \omega_s \dot{q}_s =$$

$$- \frac{E S_w^2}{\rho} \sum_{k,m,n}^{N_\Phi} \left[\sum_{l=1}^{N_\Psi} \frac{H_{m,n}^l E_{k,l}^s}{2\zeta_l^4} \right] q_k q_m q_n + p_s(t), \qquad (5)$$

The tensors appearing in Eq. (5) can be rewritten as

$$H_{i,j}^k = \frac{\int_S \Psi_k \mathcal{L}(\Phi_i, \Phi_j) \mathrm{d}S}{\|\Psi_k\| \|\Phi_i\| \|\Phi_j\|}$$

$$E_{i,j}^s = \frac{\int_S \Phi_s \mathcal{L}(\Phi_i, \Psi_j) \mathrm{d}S}{\|\Phi_s\| \|\Phi_i\| \|\Psi_j\|}.$$

and expresses the nonlinear coupling between in-plane and transverse motions. Note that in Eq. (5), the modal external force has been expressed as

$$p_s(t) = \frac{1}{\rho h S_w \|\Phi_s\|} \int_S p(\mathbf{x}, t) \Phi_s(\mathbf{x}) \mathrm{d}S.$$

In general, one may choose a separable form for $p(\mathbf{x}, t)$ and consider a Dirac delta for the space component (corresponding to pointwise forcing). Hence

$$p(\mathbf{x}, t) = \delta(\mathbf{x} - \mathbf{x}_0) P(t); \rightarrow p_s(t) = \frac{\Phi_s(\mathbf{x}_0)}{\rho h S_w \|\Phi_s\|} P(t).$$

Note also that in the same equation a modal damping term has been introduced as $2\xi_s \omega_s \dot{q}_s$. This choice is justified as metallic plates are usually only slightly damped [16].

Eq. (5) may be further simplified by introducing the fourth-order tensor $\Gamma_{j,k,l}^s$ as [13, 15]

$$\Gamma_{j,k,l}^s = \sum_{r=1}^{N_\Psi} \frac{H_{k,l}^r E_{j,r}^s}{2\zeta_r^4}. \qquad (6)$$

Remarks. System (5) is composed of N_Φ coupled Ordinary Differential Equations (ODEs). The left-hand side is the equation of a classic harmonic oscillator with loss, whereas the right-hand side is composed of a generic forcing term $p_s(t)$ plus the nonlinear coupling. This coupling involves the product of three modal coordinates and therefore for small amplitudes of vibrations (say, $w \ll h$) it becomes negligible. When $w \approx h$ the nonlinear term is responsible for weakly nonlinear phenomena, notably amplitude-dependent frequency of vibration which, thinking from the standpoint of sound synthesis, is perceived as a *pitch-bend*. Finally, when $w > h$ nonlinearities dominate the dynamics acting as a strong forcing term. Dynamically, this regime is characterised by a cascade of energy from large to small wavelengths, whose properties constitute a topic of research on its own within the realm of Wave Turbulence [4, 17, 18, 19, 20]. Typically, the cascade is perceived as a crash or a shimmering sound, and is one of the most dramatic examples of nonlinear phenomena in musical acoustics. Remarkably, these three regimes are very well described by the von Kármán equations, despite the absence of in-plane inertia. For a study on the effect of such inertia term in the von Kármán system, one may refer to [21].

3. TIME INTEGRATION

Time integration of system (5) is performed using a Störmer-Verlet scheme. For that, time is discretised according to a *sampling rate* $fs = 1/k$, where k is the time-step. Discrete time operators are now introduced. The most obvious operator is the identity operator, denoted by

$$1\mathbf{q}^n = \mathbf{q}^n.$$

Note that the notation $\mathbf{q}^n$ indicates that the vector $\mathbf{q}$ is evaluated at the discrete time kn (it must not be confused with an exponent). The backward and forward shift operators are, respectively,

$$e_{t-}\mathbf{q}^n = \mathbf{q}^{n-1}; \qquad e_{t+}\mathbf{q}^n = \mathbf{q}^{n+1}.$$

Backward, centered and forward approximations to first time derivative are defined as

$$\delta_{t-} \equiv \frac{1}{k}(1 - e_{t-}); \delta_{t\cdot} \equiv \frac{1}{2k}(e_{t+} - e_{t-}); \delta_{t+} \equiv \frac{1}{k}(e_{t+} - 1).$$

An approximation to the second time derivative can be constructed by combining the previous operators. In such a way, a particular form employed here is given by

$$\delta_{tt} \equiv \delta_{t+}\delta_{t-} = \frac{1}{k^2}(e_{t+} - 2 + e_{t-})$$

The Störmer-Verlet scheme is

$$\delta_{tt}\mathbf{q}^n + \mathbf{K}\mathbf{q}^n + \mathbf{C}\delta_{t\cdot}\mathbf{q}^n = -\mathbf{nl}^n + \mathbf{p}^n.$$

In the equation above, the matrices $\mathbf{K}$, $\mathbf{C}$ denote the normalised stiffness and damping matrices (independent of the step n). In practice, if N_Φ denoted the length of the vectors, then these matrices are $N_\Phi \times N_\Phi$; the two matrices are diagonal

$$K_{m,m} = \omega_m^2; \qquad C_{m,m} = 2\xi_m\omega_m. \tag{7}$$

The vector $\mathbf{nl}$ is the vector of the nonlinear terms, acting as a coupling. This is, simply

$$nl_m^n = \frac{ES_w^2}{\rho} \sum_{j,k,l=1}^{N_\Phi} \Gamma_{j,k,l}^m q_j^n q_k^n q_l^n. \tag{8}$$

Finally, $\mathbf{p}$ is the vector containing the forcing terms, *i.e.*

$$p_m^n = \frac{\Phi_m(\mathbf{x}_0)}{\|\Phi_m\|\rho h S_w} P^n.$$

Developing the discrete operators gives the following algebraic system, to be solved for the variable $\mathbf{q}^{n+1}$

$$\left(\frac{\mathbb{I}_{N_\Phi}}{k^2} + \frac{\mathbf{C}}{2k}\right)\mathbf{q}^{n+1} =$$
$$\left(\frac{2\mathbb{I}_{N_\Phi}}{k^2} - \mathbf{K}\right)\mathbf{q}^n + \mathbf{p}^n - \mathbf{nl}^n$$
$$+ \left(\frac{\mathbf{C}}{2k} - \frac{\mathbb{I}_{N_\Phi}}{k^2}\right)\mathbf{q}^{n-1}, \tag{9}$$

where $\mathbb{I}_{N_\Phi}$ is the $N_\Phi \times N_\Phi$ identity matrix.

Remarks. Scheme (9) is *second-order accurate* and *explicit*: the matrices multiplying the vectors are diagonal and therefore each line in the system can be solved independently (without requiring a linear system solver). This might seem puzzling at a first glance because (5) is a system of *coupled* equations. Indeed, the update of the modal scheme is composed of not only Eq. (9), but also of Eq. (8): this is where coupling happens at each update.

More generally, the Störmer-Verlet scheme is *symmetric* and *symplectic*, and is thus volume-preserving in phase space for Hamiltonian flows [22].

The associated discrete *linear* system is conservative under the Störmer-Verlet algorithm. In practice, by setting to zero the forcing ($\mathbf{p}^n$), damping ($\mathbf{C}$) and nonlinear term ($\mathbf{nl}^n$) in scheme (9), the following relation can be derived [23]

$$\delta_{t+}\sum_{s=1}^{N_\Phi} S_w^2 \frac{\rho h}{2}\left[(\delta_{t-}q_s^n)^2 + \omega_s^2 q_s^n (e_{t-}q_s^n)\right] = 0,$$

or

$$\delta_{t+}\sum_{s=1}^{N_\Phi}(\tau_s^n + \upsilon_s^n) = 0$$

which corresponds to

$$\frac{d}{dt}\sum_{s=1}^{N_\Phi} S_w^2 \frac{\rho h}{2}\left[\dot{q}_s^2(t) + \omega_s^2 q_s^2(t)\right] = 0.$$

or

$$\frac{d}{dt}\sum_{s=1}^{N_\Phi}(T_s + U_s) = 0.$$

for the continuous case. In practice, τ_s^n and υ_s^n are the corresponding discrete kinetic and potential energies of the linear plate, which can be seen as the sum of uncoupled harmonic oscillators.

Conservation of discrete energy allows to derive a stability condition for the scheme applied to the linear plate equation. Let $\hat{\omega}_s$ denote the largest eigenfrequency of the system, then the scheme is stable when [23]

$$\hat{k} < \frac{2}{\hat{\omega}_s}. \tag{10}$$

$$\begin{pmatrix} a_{11} & a_{12} & a_{13} & ... & a_{1N} \\ a_{21} & a_{22} & a_{23} & ... & a_{2N} \\ \vdots & \vdots & \ddots & ... & \vdots \\ a_{M1} & a_{M2} & a_{M3} & ... & a_{MN} \end{pmatrix} \begin{pmatrix} v_1 \\ v_2 \\ \vdots \\ v_M \end{pmatrix} = \begin{pmatrix} c_1 \\ c_2 \\ \vdots \\ c_M \end{pmatrix}$$

Figure 1: Parallel structure of update (8) for the nonlinear term. Each colour represents an operation that can be solved independently in a parallel environment.

When this condition is enforced, then the discrete energies are positive definite and the scheme is stable (*i.e.* the solutions are bounded over time). This *same* condition can be extended to the nonlinear system when the time integration scheme proposed in [8] is applied. The resulting algorithm, however, becomes implicit and the computational time increases.

A second remark has to do with the efficiency of the scheme. Most time is spent in updating the nonlinear term, (8). However, such an update presents a highly parallel structure, being basically a series of products of matrices (see fig. 1). In MATLAB, matrix multiplication is automatically assigned to multiple cores when possible, but in theory many more (and faster) possibilities are open to anyone wishing to port the modal code to other languages (C, CUDA, etc.).

4. CASE STUDIES

System (5) is completely general, meaning that the integration scheme (9) can be applied as long as the coupling coefficients (6) are known together with the radian frequencies in Eq. (2). In general, analytic solutions are not available for given geometry and boundary conditions, but there are important cases which constitute an exception. Two of such cases are presented now: a circular plate with free boundary and a rectangular plate with simply supported boundary.

4.1. Free Circular Plate

A circular plate of radius a with a free edge is first considered. The boundary conditions then read, for the two unknowns $w(r, \theta, t)$ and $F(r, \theta, t)$ [24] (an index after a comma indicates a derivative in that direction)

$$\forall t, \ \forall \theta \in [0, 2\pi], \ \text{at} \quad r = a :$$
$$w_{,rr} + \frac{\nu}{a} w_{,r} + \frac{\nu}{a^2} w_{,\theta\theta} = 0 ,$$
$$w_{,rrr} + \frac{1}{a} w_{,rr} - \frac{1}{a^2} w_{,r} + \frac{2-\nu}{a^2} w_{,r\theta\theta} - \frac{3-\nu}{a^3} w_{,\theta\theta} = 0 ,$$

$$F_{,r} + \frac{1}{a} F_{,\theta\theta} = 0 , \quad F_{,r\theta} + \frac{1}{a} F_{,\theta} = 0 .$$

Despite a seemingly complex form of the boundary conditions, an analytical solution exists in the form of Bessel functions. The eigenfrequencies are then obtained as the zeros of such functions. The eigenfunctions are here denoted by either a single integer number p - sorting the frequencies from small to large - or by a pair (k_c, k_d), where k_c denotes the number of nodal diameters and k_d the number of nodal circles. As it is usual with circular symmetry, asymmetric modes with $k_c \neq 0$ are degenerated so that two

CIRCULAR PLATE

mode label p	$\bar{\omega}_p$	$\bar{\Gamma}^p_{p,p,p}$	N^{conv}_{Ψ}
1,2	1	$1.90 \cdot 10^0$	3
3	1.8	$8.58 \cdot 10^0$	4
4,5	2.3	$1.70 \cdot 10^1$	4
715,716	527.7	$8.44 \cdot 10^6$	65
846	627.6	$2.86 \cdot 10^6$	36
881,882	658.1	$1.78 \cdot 10^6$	50

RECTANGULAR PLATE

mode label p	$\bar{\omega}_p$	$\bar{\Gamma}^p_{p,p,p}$	N^{conv}_{Ψ}
1	1	$2.00 \cdot 10^1$	12
20	13.9	$9.50 \cdot 10^3$	286
72	48.1	$1.07 \cdot 10^5$	239
336	208.7	$2.50 \cdot 10^6$	25
422	261.5	$5.88 \cdot 10^6$	103
589	361.9	$1.23 \cdot 10^7$	132

Table 1: Convergence of the nondimensional coupling coefficients $\bar{\Gamma}^p_{p,p,p}$ for the circular plate and a rectangular plate with aspect ratio $2/3$. Modes are sorted according to increasing eigenfrequency. N^{conv}_{Ψ} indicates *upper bounds* of the number of in-plane modes needed for displayed accuracy. The normalised eigenfrequencies $\bar{\omega}_p$ are also shown.

eigenvectors are found for the same eigenfrequency. For the circular plate, eigenfrequencies for both the transverse and in-plane problems are analytic so that the numerical values of $\{\omega_i, \zeta_j\}_{i,j\geq 1}$ used to feed the model can be considered exact. In the truncation process, the number of in-plane modes N_{Ψ} may be selected according to the desired accuracy for the cubic coupling coefficient $\Gamma^p_{p,p,p}$ defined in Eq. (6), see *e.g.* [24, 15, 25]. As explained in [24], some specific rules exist, so that, for a given transverse mode p, only a few in-plane modes participate with a non-vanishing contribution to the summation in Eq. (6). The rules are as follows:

- For a purely axisymmetric mode $\Phi_{(0,k_d)}$, only the axisymmetric in-plane modes $\{\Psi_{(0,i)}\}_{i\geq 1}$ participate to the summation.

- For an asymmetric mode $\Phi_{(k_c,k_d)}$ with $k_c \neq 0$, then the coupling involve only axisymmetric in-plane modes $\{\Psi_{(0,i)}\}_{i\geq 1}$ as well as asymmetric in-plane modes having twice the number of nodal diameters $\{\Psi_{(2k_c,i)}\}_{i\geq 1}$.

Hence for a given mode p, the convergence of the summation for $\Gamma^p_{p,p,p}$ is achieved within a small subset of all the possible in-plane modes. Let N^{conv}_{Ψ} be the cardinal of this subset of admissible modes. The convergence of three coefficients $\Gamma^p_{p,p,p}$ is shown in Fig. 2, for three different modes of high frequencies. It is seen that convergence is assured even for such high-order coefficients. An axisymmetric mode with a many nodal circles, mode (0,18) has been selected together with a purely asymmetric one, mode (50,0), and a mixed mode : (24,8). Table 1 presents the converged values of a few nondimensional coefficients. For asymmetric modes (k_c, k_d) with $k_c \neq 0$, the modes are degenerate.
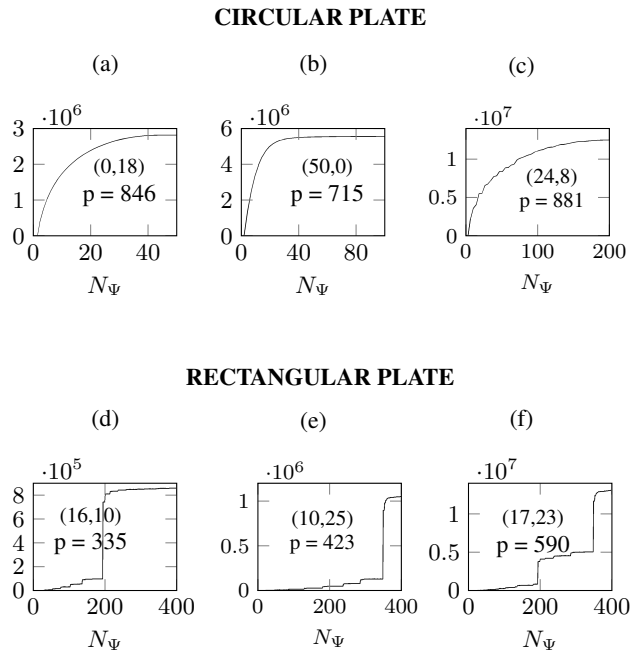
CIRCULAR PLATE

RECTANGULAR PLATE

Figure 2: Plots of a few nondimensional values of coupling coefficients, $\bar{\Gamma}^p_{p,p,p}$. (a)-(c): Circular plate. Numbers in brackets are (k_c, k_d) corresponding to nodal circles and diameters. (e)-(f): Rectangular plate of aspect ratio 2/3. Numbers in brackets are (k_1, k_2) of Eq. (12).

4.2. Simply-Supported Rectangular Plate

Consider a rectangular plate of lateral dimensions L_x, L_y. Let n, t denote the normal and tangential directions to the boundary δS. Simply-supported boundary conditions may be given as

$$\forall t, \ \forall \mathbf{x} \in \delta S :$$
$$w = w_{,nn} + \nu w_{,tt} = 0,$$
$$F_{,nt} = F_{,tt} = 0. \tag{11}$$

Such conditions, despite not describing a load-free edge (a desirable case for sound synthesis), have the advantage of being particularly simple. The solution for the transverse modes, in fact, is given in terms of sine functions [14]

$$\Phi_k(\mathbf{x}) = \sin \frac{k_1 \pi x}{L_x} \ \sin \frac{k_2 \pi y}{L_y} \qquad \text{for integers } k_1, \ k_2.$$

The eigenfrequencies are then easily obtained as

$$\omega_k^2 = \frac{D}{\rho h} \left[\left(\frac{k_1 \pi}{L_x} \right)^2 + \left(\frac{k_2 \pi}{L_y} \right)^2 \right]^2 . \tag{12}$$

The conditions for the in-plane function, on the other hand, can be worked out to yield a simplified form. Consider in fact the following conditions

$$F = F_{,n} = 0 \quad \forall \mathbf{x} \in \delta S;$$

it is clear that these conditions are sufficient (but not necessary) to satisfy (11) [13]. Such conditions, along with Eq. (3), reduce the

quest for the eigenfunctions Ψ_k to the clamped plate problem. Despite not having a closed-form solution, this problem was recently shown to have a semi-analytical solution based on the Rayleigh-Ritz method, yielding ~ 400 eigenfunctions and associated frequencies with precision to, at least, four significant digits [15]. As opposed to the circular case, it is difficult to have an *a priori* knowledge on the coupling rules. This is because the form of the in-plane eigenfunctions is not known analytically, and thus only a numerical investigation can help in laying out coupling rules. As for the circular case, coefficients of the kind $\Gamma^p_{p,p,p}$ are investigated. In general, when either k_1 or k_2 is small, convergence is quite fast, see for example fig. 2(f). However, modes for which neither k_1 or k_2 is small, convergence is much slower and presents a staircase-like behaviour, like in fig. 2(d). Nonetheless, table 1 shows accuracy to a few decimal digits is still assured even for coefficients involving high-frequency modes.

Remarks. Table 1 shows the convergence of the nonlinear coupling coefficients. With respect to other numerical techniques, namely Finite Differences, such order of convergence is out-of-reach for reasonable sample rates [15]. This remark should be kept in mind when comparing the *efficiency* (or numerical burden) of the modal method versus a Finite Difference scheme: for the same degree of accuracy, Finite Differences are much less efficient than modes.

On the other hand, the two case studies presented here are somewhat an exception as they have analytical or semi-analytical solutions for the modes. When facing a case for which the modes are not known, the modal approach becomes somewhat less appealing than other numerical methods.

5. SIMULATIONS

Now that the coupling coefficients are eigenfrequencies have been calculated for the case studies, scheme (9) may be applied. First, excitation and loss are presented, and then results of simulations shown.

5.1. Excitation

For pointwise forcing, two different excitation mechanisms will be considered here: 1. a strike and 2. a sinusoidal forcing.

Strikes are of course the most direct way to excite a plate. In general, one wishes to have control on the "loudness" and "brilliance" of the sound. To a first approximation, these parameters may be controlled by making use of a relatively simple form for the excitation, a raised cosine. This function is defined as

$$P(t) = \begin{cases} \frac{\bar{P}}{2} \left[1 + \cos \left(\pi (t - t_0)/T_{wid} \right) \right] & \text{if } |t - t_0| \leq T_{wid} ; \\ 0 & \text{if } |t - t_0| > T_{wid} . \end{cases}$$

It is seen that one has control over two parameters: T_{wid}, or half of the total contact duration, and $\bar{P}$, the maximum amplitude. As a rule of thumb, one may use a shorter T_{wid} and a larger $\bar{P}$ to increase the "loudness" and "brightness" of the output. See also fig. 3(a).

Sinusoidal forcing (see fig. 3(b)) may instead by applied to observe the system undergo two bifurcations, leading first to a quasi-periodic and then to a turbulent motion. Perceptually, the three regimes are very well recognisable ranging from an almost monochromatic sound to a loud, shimmering cascade.
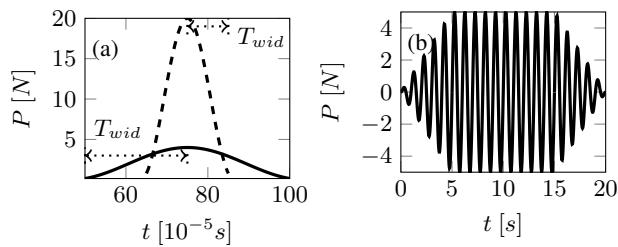
Figure 3: (a): examples of raised cosine functions used to simulate a strike, in the case of "hard" contact (dashed) and "soft" contact (thick). (b): example of sinusoidal forcing of frequency 1Hz and amplitude 5N increased linearly to a steady value and then decreased.
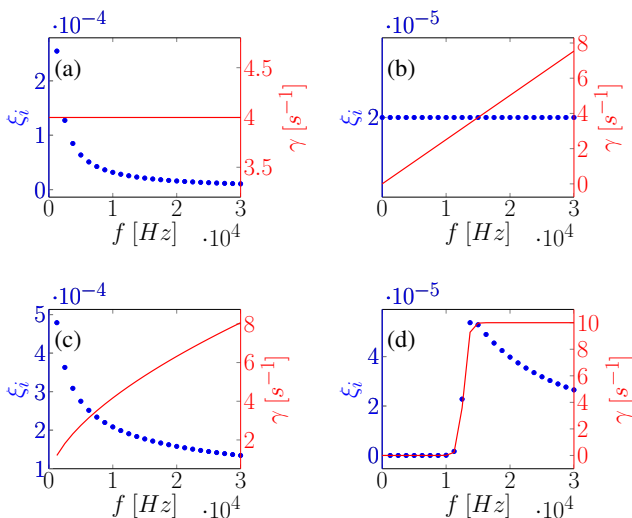

Figure 4: Examples of damping coefficients $\xi_i(\omega)$ (dots) and resulting damping laws $\gamma(\omega) = 2\xi_i\omega_i$ (thick lines). (a): $\xi_i = 2/\omega_i$. (b): $\xi_i = 2 \cdot 10^{-5}$. (c): damping law as measured by Humbert [26] for a plate of thickness $h = 0.5$mm, $\xi_i = 8 \cdot 10^{-3}\omega_i^{-0.4}$. (d): $\xi_i = 5/[\omega_i(\exp(32 - \omega_i/2500) + 1)]$.

5.2. Loss

For sound synthesis, loss bears about a lot of perceptual information. One of the advantages of the modal approach is that a complex decay can be simulated by setting by hand the modal damping coefficients ξ_m in Eq. (7). For example, if one wishes to simulate a damping law which dissipated energy at the same rate at all scales, one may set $\xi_m = c/\omega_m$; a linear damping law is obtained for $\xi_m = c$ for constant c. Of course, the possibilities are endless, see also fig. 4

5.3. Examples

Fig. 6 reports the simulations for three different cases: 1. a soft strike; 2. a hard strike; 3. a sinusoidally forced plate. For nonlinear dynamics, in the case of a strike, the pictorial example of fig. 5 shows one snapshot immediately after a strike and one at later moment when the profile is fully turbulent.

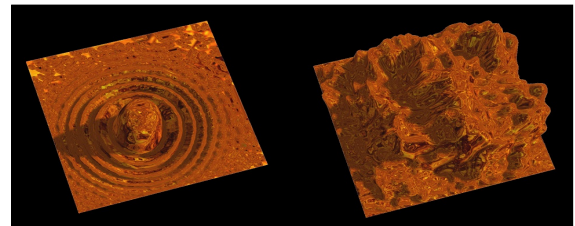The plate under consideration is a small rectangular plate of

Figure 5: Snapshots of displacement field on top of a plate just after a strike (left) and during fully developed nonlinear state (right), with the presence of large and small wavelengths.

dimensions 21cm× 18cm × 1mm. For this plate, the eigenfrequencies are such that $\omega_{250}/2\pi = 21610$Hz, suggesting that even a relatively small number of modes suffices to reproduce a rich sound spanning a large interval of the audible range. The output can be extracted by recording the displacement at one point on the plate, w_0^n, and by taking a discrete time derivative in order to high-pass the frequency spectrum.

Because instability may set in, one must set the sampling frequency to a reasonably high rate in order to obtain convergence. The reference sampling rate in this case is given by Eq. (10), which gives the stability condition for the linear plate. Because in this case the dynamics is nonlinear, one has to guess a value of the sampling rate which assures convergence, but which remains sufficiently small in order to allow fast computations. Empirically, it is found that for

$$k_{\text{sim}} = \hat{k}/2$$

the solution converges even for a strongly nonlinear dynamics (at least for vibrations up to $2-3$ times the thickness) and hence such is the time-step selected for the simulations.

Fig. 6(a)-(b) is the typical case of weakly nonlinear vibrations, with amplitude $w \sim h$. To simulate a soft strike using a raised cosine, the particular parameters employed here are $T_{wid} = 1$ms, $\bar{P} = 100$N. The damping coefficients are set as $\xi_i = 8 \cdot 10^{-3}\omega_i^{-0.4}$. The total number of modes retained is fairly small, $N_\Phi = 100$, covering frequencies up to 9000Hz. The number of in-plane modes is $N_\Psi = 50$. In this case, the modes are weakly coupled giving rise to pitch-bends and amplitude-dependent frequency of vibration. The damping law selected allows to simulate a very enjoyable decay, with complex auditory cues.

Fig. 6(c)-(d) represents the case of strong nonlinear dynamics. The plate is activated by a raised cosine with $T_{wid} = 0.8$ms, $\bar{P} = 300$N. Damping coefficients and number of modes are the same as for the previous case. Here, the amplitude of vibrations has a maximum at $2h$, indicating that more nonlinear phenomena may set in. In fact, by looking at the velocity spectrogram one can notice that just after the strike the modes are not very well distinguishable: this is a trace of a turbulent dynamics corresponding to a shimmering sound typical of gongs. After this initial transient, loss removes energy from the system until the modes are again perfectly distinguishable, and eventually killed.

Perhaps the most interesting case is represented in fig. 6(e)-(f). In this case the plate is activated by a sinusoid close to the 5th eigenfrequency of the system. The amplitude of the sinusoid is increased from 0 to 116N in 1s, then kept steady for 5s and eventually decreased to zero in 2s. The plate undergoes 2 bifurcations denoted in the spectrogram by thick dashed lines: at the
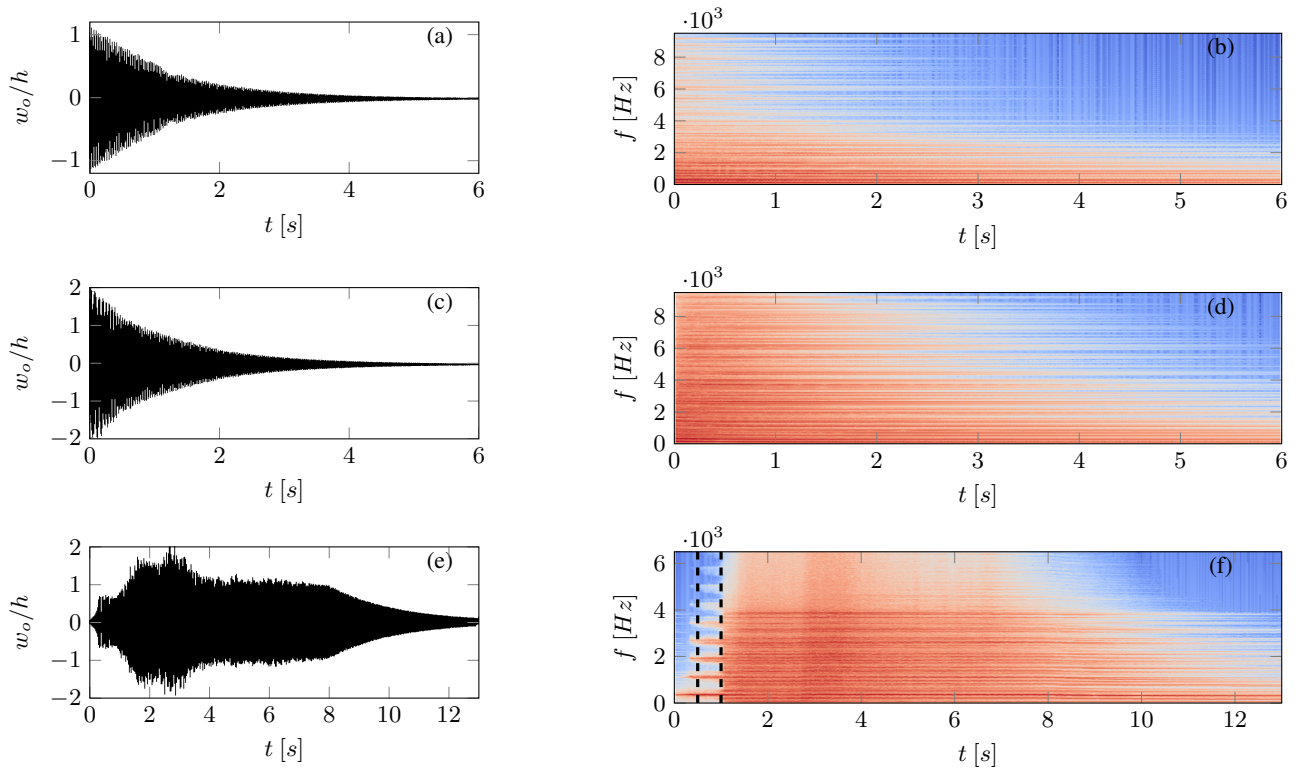
Figure 6: Numerical simulations of a rectangular plate with dimensions 21cm× 18cm × 1mm. (a)-(b): Time series of displacement and velocity spectrogram of "soft" strike, with $\bar{P} = 100$N, $T_{wid} = 1$ms, $\xi_i = 8 \cdot 10^{-3}\omega_i^{-0.5}$, $N_\Psi = 50$, $N_\Phi = 100$. (c)-(d): Time series of displacement and velocity spectrogram of "hard" strike, with $\bar{P} = 300$N, $T_{wid} = 0.8$ms, $\xi_i = 8 \cdot 10^{-5}\omega_i^{-0.4}$, $N_\Psi = 50$, $N_\Phi = 100$. (e)-(f): Time series of displacement and velocity spectrogram of sinusoidally forced plate, with sinusoid of frequency $1.02 f_5$ and maximum amplitude 116N, increased linearly for 1s, kept steady for 5s, and then decreased to zero in 2s; $\xi_i = 4 \cdot 10^{-3}\omega_i^{-0.4}$, $N_\Phi = 72$, $N_\Psi = 60$; dashed lines on spectrogram indicate bifurcations from a linear regime, to a quasi-periodic regime, to a turbulent regime.

start one can clearly hear a monochromatic sound at the selected frequency; after the first bifurcation the same frequency is modulated by higher harmonics; and after the second bifurcation all the modes are activated in a turbulent bath. The damping law selected are able to give the sound a natural richness with complex harmonic relations.

Calculation times in MATLAB are quite fast. For the strikes (*i.e.* $N_\Psi = 50$, $N_\Phi = 100$, $k_{\text{sim}} = \hat{k}/2$) the calculation time is about 8 times real-time, on a machine equipped with an Intel i7 CPU at 2.40GHz. For the sinusoid (*i.e.* $N_\Psi = 50$, $N_\Phi = 60$, $k_{\text{sim}} = \hat{k}/2$) the calculation time is about 1.5 times real-time.

6. CONCLUSIONS

This work presented an explicit modal scheme for the nonlinear plate equations. For the cases which present a semi-analytic solution for the modes, it was shown that the eigenfrequencies and coupling coefficients can be calculated to a very high precision. The modal update is completely general as long as such frequencies and coefficients are known. Two case studies were presented, including the important case of a circular plate with a free boundary. Numerical simulations were provided to show that the modal scheme can simulate efficiently a complex dynamics, resulting in very realistic sound synthesis.

7. REFERENCES

[1] A. H. Nayfeh, *Nonlinear interactions: analytical, computational and experimental methods*, Wiley series in nonlinear science, New-York, 2000.

[2] M. Amabili, *Nonlinear vibrations and stability of shells and plates*, Cambridge University Press, 2008.

[3] C. Touzé, S. Bilbao, and O. Cadot, "Transition scenario to turbulence in thin vibrating plates," *Journal of Sound and Vibration*, vol. 331, no. 2, pp. 412–433, 2012.

[4] G. Düring, C. Josserand, and S. Rica, "Weak turbulence for a vibrating plate: Can one hear a Kolmogorov spectrum?," *Physical Review Letters*, vol. 97, pp. 025503, 2006.

[5] S. Bilbao, *Numerical Sound synthesis: Finite Difference Schemes and Simulation in Musical Acoustics*, Wiley, 2009.

[6] A. Chaigne and V. Doutaut, "Numerical simulations of xylophones. i. time-domain modeling of the vibrating bars," *The Journal of the Acoustical Society of America*, vol. 101, no. 1, 1997.

[7] C. Lambourg, A. Chaigne, and D. Matignon, "Time-domain simulation of damped impacted plates. II: Numerical model and results," *The Journal of the Acoustical Society of America*, vol. 109, no. 4, 2001.

[8] S. Bilbao, "A family of conservative finite difference schemes for the dynamical von Kármán plate equations," *Numerical Methods for Partial Differential Equations*, vol. 24, no. 1, pp. 193–216, 2007.

[9] A. Torin and S. Bilbao, "A 3D multi-plate environment for sound synthesis," in *Proceedings of the 16th International Conference on Digital Audio Effects*, 2013.

[10] J. Chadwick, S. An, and D. James, "Harmonic shells: a practical nonlinear sound model for near-rigid thin shells," *ACM Transactions on Graphics (SIGGRAPH ASIA Conference Proceedings)*, vol. 28, no. 5, pp. Article 119, 2009.

[11] M. Ducceschi and C. Touzé, "Modal approach for nonlinear vibrations of damped impacted plates: Application to sound synthesis of gongs and cymbals," *Journal of Sound and Vibration*, vol. 344, pp. 313 – 331, 2015.

[12] L.D. Landau and E.M. Lifschitz, *Theory of Elasticity, Third Edition*, Elsevier Butterworth Heinemann, 1986.

[13] O. Thomas and S. Bilbao, "Geometrically nonlinear flexural vibrations of plates: In-plane boundary conditions and some symmetry properties," *Journal of Sound and Vibration*, vol. 315, no. 3, pp. 569–590, 2008.

[14] P. Hagedorn and A. DasGupta, *Vibrations and Waves in Continuous Mechanical Systems*, Wiley, 2007.

[15] M. Ducceschi, C. Touzé, S. Bilbao, and C.J. Webb, "Nonlinear dynamics of rectangular plates: investigation of modal interaction in free and forced vibrations," *Acta Mechanica*, vol. 225, no. 1, pp. 213–232, 2014.

[16] J. Woodhouse, "Linear damping models for structural vibration," *Journal of Sound and Vibration*, vol. 215, no. 3, pp. 547 – 569, 1998.

[17] A. Boudaoud, O. Cadot, B. Odille, and C. Touzé, "Observation of wave turbulence in vibrating plates," *Physical Review Letters*, vol. 100, pp. 234504, 2008.

[18] N. Mordant, "Are there waves in elastic wave turbulence ?," *Physical Review Letters*, vol. 100, pp. 234505, 2008.

[19] P. Cobelli, P. Petitjeans, A. Maurel, V. Pagneux, and N. Mordant, "Space-time resolved wave turbulence in a vibrating plate," *Physical Review Letters*, vol. 103, pp. 204301, 2009.

[20] M. Ducceschi, O. Cadot, C. Touzé, and S. Bilbao, "Dynamics of the wave turbulence spectrum in vibrating plates: A numerical investigation using a conservative finite difference scheme," *Physica D*, vol. 280-281, pp. 73–85, 2014.

[21] S. Bilbao, O. Thomas, C. Touzé, and M. Ducceschi, "Conservative numerical methods for the full von Kármán plate equations," *Numerical Methods for Partial Differential Equations*, (accepted for publication) 2015.

[22] E. Hairer, C. Lubich, and G. Wanner, *Geometric numerical integration: structure-preserving algorithms for Ordinary differential equations*, Springer, 2006, second edition.

[23] M. Ducceschi, *Nonlinear vibrations of thin rectangular plates. A numerical investigation with application to wave turbulence and sound synthesis*, Ph.D. thesis, Ecole doctorale de l'Ecole Polytechnique, 2014.

[24] C. Touzé, O. Thomas, and A. Chaigne, "Asymmetric nonlinear forced vibrations of free-edge circular plates, part I: theory," *Journal of Sound and Vibration*, vol. 258, no. 4, pp. 649–676, 2002.

[25] C. Touzé, M. Vidrascu, and D. Chapelle, "Direct finite element computation of non-linear modal coupling coefficients for reduced-order shell models," *Computational Mechanics*, vol. 54, no. 2, pp. 567 – 580, 2014.

[26] T. Humbert, O. Cadot, G. Düring, C. Josserand, S. Rica, and C. Touzé, "Wave turbulence in vibrating plates: The effect of damping," *EPL (Europhysics Letters)*, vol. 102, no. 3, pp. 30002, 2013.